The International Journal of Advanced Manufacturing Technology (2020) 110:2703–2711
https://doi.org/10.1007/s00170-020-06031-0

ORIGINAL ARTICLE

Effect of processing parameters on corrosion behaviour of Al reinforced with Ni-40Fe-10Ti alloy fabricated by FSP

T. H. Sibisi[1] · M. B. Shongwe[1] · O. T. Johnson[2] · R. M. Mahamood[3,4] · S. A. Akinlabi[5] · S. Hassan[5] · H. Dong[6] · K. F. Carter[7] · E. T. Akinlabi[8]

Received: 18 April 2020 / Accepted: 1 September 2020 / Published online: 12 September 2020

Abstract

Aluminium alloys has been favoured in many applications because of its exciting properties which include light weight and corrosion resistance. However, susceptibility to pitting corrosion and intergranular corrosion (IGC) are some of the drawbacks of aluminium. The surface of aluminium can be modified to improve its corrosion resistance properties. Surface modification is a surface engineering process that is performed to alter the properties of material surface to improve its service life. Friction stir processing (FSP) is a relatively new and an important solid state material surface modification process. In this study, investigation on the influence of FSP processing parameters on the resulting corrosion resistance surface properties of pure commercial aluminium and Ni-40Fe-10Ti surface composite using friction stir processing technique was conducted. The processing parameters that were studied are tool rotational speed and transverse speed, while all other processing parameters were kept constant. The corrosion behaviour was studied using three-electrode electrochemical cell, and the microstructure of the corroded samples was studied using optical microscope (OM). The results showed that the addition of Ni, Fe and Ti caused a decrease in the anodic and cathodic current densities. The set of processing parameters that resulted in the lowest corrosion rate are the rotational speed of 600 rpm and transverse speed of 70 mm/min.

Keywords Aluminium · Friction stir processing · Corrosion · Microstructure · Processing parameter

✉ R. M. Mahamood
mahamoodmr2009@gmail.com

[1] Department of Chemical, Metallurgical & Materials Engineering, Tshwane University of Technology, P.M.B. X680, Pretoria, South Africa

[2] Department of Mining and Metallurgical Engineering, University of Namibia, Ongwediva Campus, P O Box 3624, Ongwediva, Namibia

[3] Department of Materials and Metallurgical Engineering, University of Ilorin, Ilorin, Nigeria

[4] Department of Mechanical Engineering Science, University of Johannesburg, Auckland Park, P O Box 524, Johannesburg 2006, South Africa

[5] Department of Mechanical Engineering, Walter Sisulu University, Butterworth Campus, Butterworth, South Africa

[6] Materials Innovation Centre, School of Engineering, University of Leicester, Leicester, UK

[7] Engineering Department, University of Leicester, Leicester, UK

[8] Pan Africa University for Earth and Life Sciences, Ibadan, Nigeria

1 Introduction

Aluminium and its alloys are mostly used in submarine, automobile and aerospace industries as a result of good corrosion resistance properties and light weight they possess [1]. Despite these exciting properties, the most aluminium and its alloys are susceptible to localized corrosions such as pitting corrosion and intergranular corrosion (IGC) [2]. Properties or the behaviour of aluminium and its alloys depends mainly on the microstructural structures [3, 4]. By modifying the microstructural make-up of aluminium and its alloy through surface modification techniques, the resistance of this material to IGC and pitting corrosion can be improved.

There are several surface modification techniques that are reported in the literature for improving the surface properties of materials that include the production of metal matrix composite on the surface of the material. Aluminium metal composites (MMC's) surface modification can be achieved using different surface engineering processes that include high-energy laser surface alloying, powder metallurgy and plasma spraying [5]. The inherent porosity in liquid state processing

Table 1 Experimental matrix

Sample designation	The rotational (rpm)	Transverse speeds (mm/min)
A	600	70
B	600	140
C	600	210
D	800	70
E	800	140
F	800	210
G	1000	70
H	1000	140
I	1000	210

and limited achievable strength of powder metallurgy has restricted their use in many applications. In addition to that, laser alloying and plasma spraying techniques are characterized with poor solidification and cracking that is caused by porosity when used with aluminium and its alloys because the process involve high-temperature liquid phase processing [6, 7]. In order to reduce or eliminate the aforementioned problems, solid state surface processing of aluminium and its alloys which is done below its melting temperature will yield a better result. There is an increasing demand for new surface processing techniques for aluminium and its alloy that is done in solid state such as friction stir processing [8].

Friction stir processing (FSP) is a solid state surface modification technique that was introduced by Mishra and Ma [9]. This FSP is a technology that is based on friction stir welding technique invented in 1991 by TWI and has since been used as surface modification technique for aluminium and its alloys [10]. The advantages offered by FSP include microstructural refinement, elimination of defects, grain homogeneity at the processed zone and densification [11–14]. The literature is scarce on studying of the effect of rotational and transverse speeds on the corrosion properties of friction stir processed (FSPed) pure commercial aluminium composite. Against this background, the role of FSP process parameters (tool rotational speed and transverse speed) in the improvement of localized corrosion susceptibility of FSPed pure commercial aluminium reinforced with Ni-40Fe-10Ti alloy was investigated in this study. This study is important because localized corrosion on manufactured part is a favourable site crack initiation because of high concentration factor they offer that eventually results in premature failure of material in service.

2 Experimental procedure

Five millimetre thick as-received pure commercial aluminium was used as the substrate material in this investigation. The substrate was wire cut into strips of dimension 245 mm × 200 mm × 5 mm. The reinforcement materials used in this study Ni, Fe and Ti powders with particle sizes used ranged between 2.2 and 36 μm and was supplied by Wear Tech (PTY) limited, South Africa. The elemental powders were first thoroughly mixed using the mixing ratio by weight of 50% Ni, 40% Fe and 10% Ti before being incorporated into the substrate. The commercial Ni powder is the main component of the reinforcement alloy which is made up of 50% by weight of the total reinforcement powders. Fifty percent of nickel, 40% of iron and 10% of titanium powders were mixed for 6 h to ensure uniform distribution of the reinforcement powders using tubular mixer at the rotational speed of 101 rpm. The groove filling method was adopted for the friction stir processing. A tool of tool pin 3 mm diameter was plunged into 3 mm depth on the substrate to create the grooves. Before the FSP, a groove of dimension 3 mm × 3 mm was cut in the middle of the substrate spanning the length of 210 mm

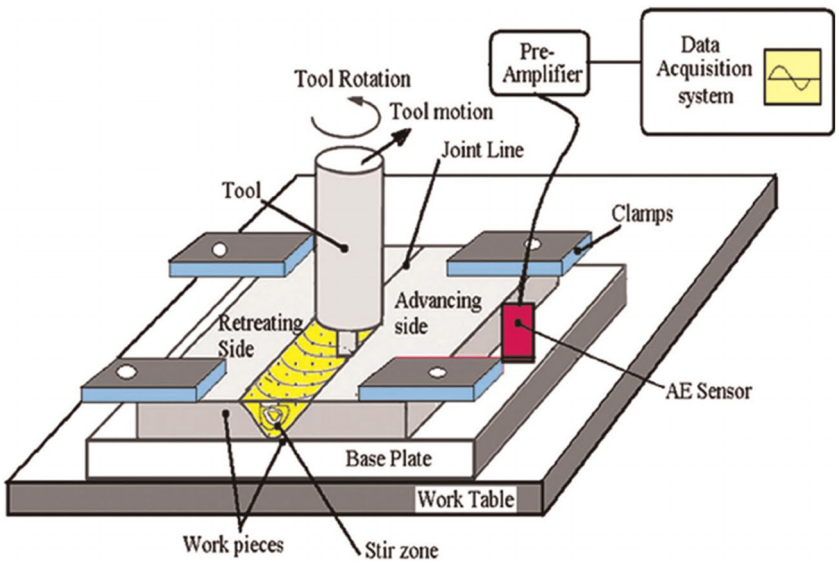

Fig. 1 Schematic diagram of FSP

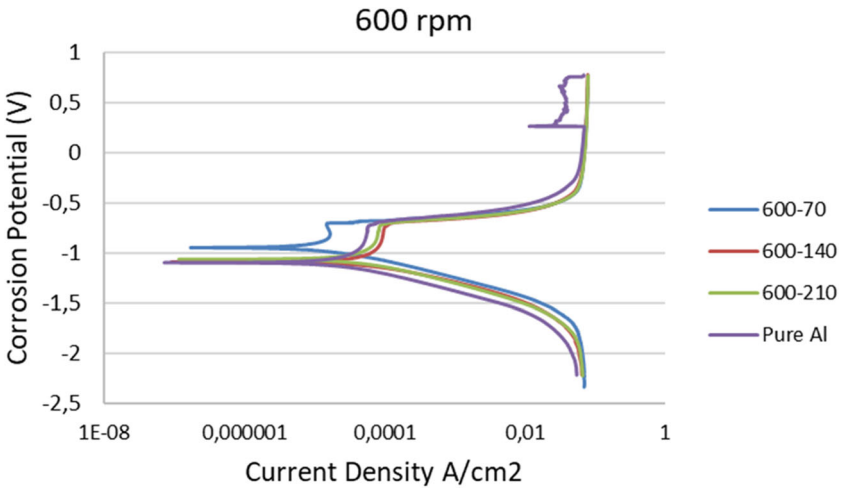

Fig. 2 Potentiodynamic polarization curves for FSPed samples produced at 600 rpm and pure Al in 3.5% NaCl

leaving 20 mm to the edge of the substrate before starting the groove. The mixed reinforcement powder was then incorporated to fill the groove. Reinforcement of volume of 1.89×10^{-6} mm^3 was incorporated to each substrate and maintained throughout the experiments. To prevent the reinforcement powder from leaving the grove during the FSP, the groove opening was closed off using a flat shoulder pin-less tool. The tool employed for the FSP in this study has a shoulder diameter of 18 mm, pin diameters of 3 mm and pin length of 4 mm and was made of M-35 high speed steel (HSS). The tool rotational speed was varied between 600 and 1000 rpm, while the transverse speed was varied between 70 and 210 mm/min, and the tool tilt angle was maintained at 3°

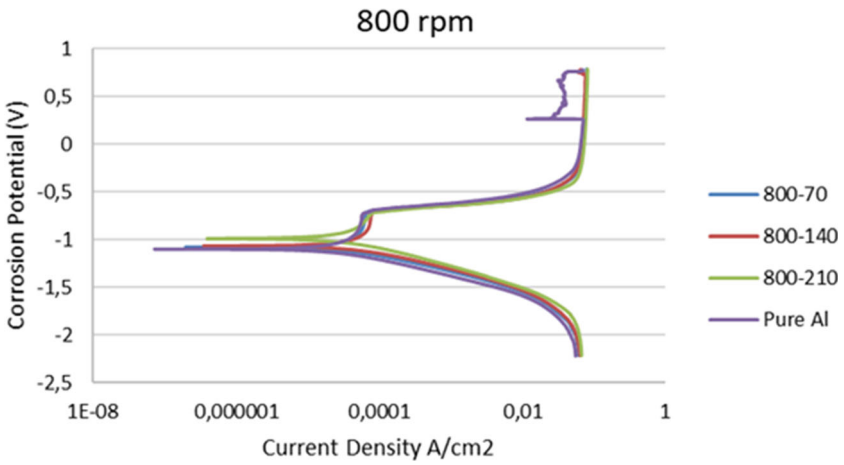

Fig. 3 Potentiodynamic polarization curves of FSPed sample processed at 800 rpm in 3.5% NaCl

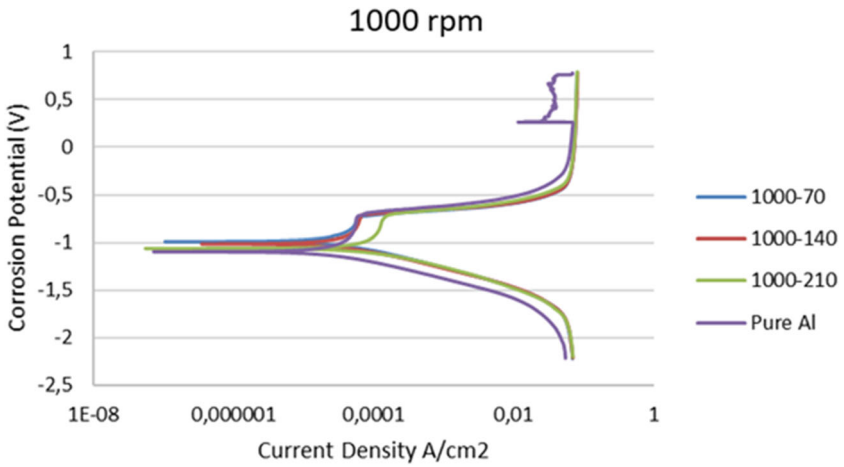

Fig. 4 Potentiodynamic polarization curves for base metal and FSPed samples produced at 1000 rpm in 3.5% NaCl

Table 2 Corrosion results

Rotational speed (rpm)	Transverse speed (mm/min)	Ecorr (V)	jcorr (A/cm^2) (10^{-6})	CR (mm/year)	PR (Ω)
600	70	− 0.94785	43.5	1.2176	3079.9
600	140	− 1.0904	115	3.2191	2030.2
600	210	− 1.0645	105	2.9547	1633.6
800	70	− 1.0789	104	2.9129	1093.1
800	140	− 1.064	78.9	2.2107	1453.9
800	210	− 1.064	628	17.596	176.58
1000	70	− 0.98843	207	5.8085	783.14
1000	140	− 1.0167	235	6.573	913.76
1000	210	− 0.98843	207	5.8085	783.14
Pure Al	–	− 1.0983	232	6.4881	1770.7

from the plate normal direction. Other processing parameters were kept at constant values throughout the experiments. The experimental matrix employed in this study is presented in Table 1. The friction stir processing was then performed. The schematic diagram of friction stir processing is shown in Fig. 1. The tool used is a nonconsuming rotating tool with the pin and shoulder plunged into the workpiece until the tool shoulder was in close contact with the workpiece and then the FSP progresses. A lot of heat is generated on the surface because of the friction between the rotating tool and the workpiece which then causes severe plastic deformation of the base metal. The plasticized based metal are forced to be mixed with the reinforcement powder particles as the tool rotates and transverse through the workpiece.

The corrosion test was conducted in corrosive medium of 3.5% NaCl solution using a three-electrode electrochemical cell system at 25 ± 1 °C. Experimental equal dimension of 1 cm × 1 cm surface dimension coupons was cut from the FSPed samples. Covered copper wire was attached to each of the samples and cold mounted in an epoxy resin. The mounted samples were wet grounded to P320 grit SiC. To obtain information on the corrosion behaviour of FSPed samples, pure commercial aluminium incorporated with Ni-40Fe-10Ti alloy, Auto-lab potentiostat PGSTAT30 was employed to conduct open-circuit potential (OCP) and cyclic potentiodynamic polarization tests. Ag/AgCl saturated with 3 M KCl was used as reference electrode, and graphite rod was used as counter electrode and the FSPed specimens as the working electrode. OCP test was conducted for 1 h, while the polarization measurements were conducted at a scan rate of 1 mV s^{-1} and potentially initiated at − 1.5 to + 1.5 V. The corroded samples were studied using optical microscope.

3 Results and discussions

Corrosion results obtained from the polarization curves are corrosion potential (Ecorr), and corrosion current density (Icorr) using Tafel extrapolation method (Figs. 2, 3, and 4) are presented in Table 2.

The potentiodynamic polarization curves of the pure commercial aluminium and that of the FSPed Al/Ni-40Fe-10Ti composites that were produced at rotational speed of 600 rpm and at varying transverse speeds are shown in Fig. 2.

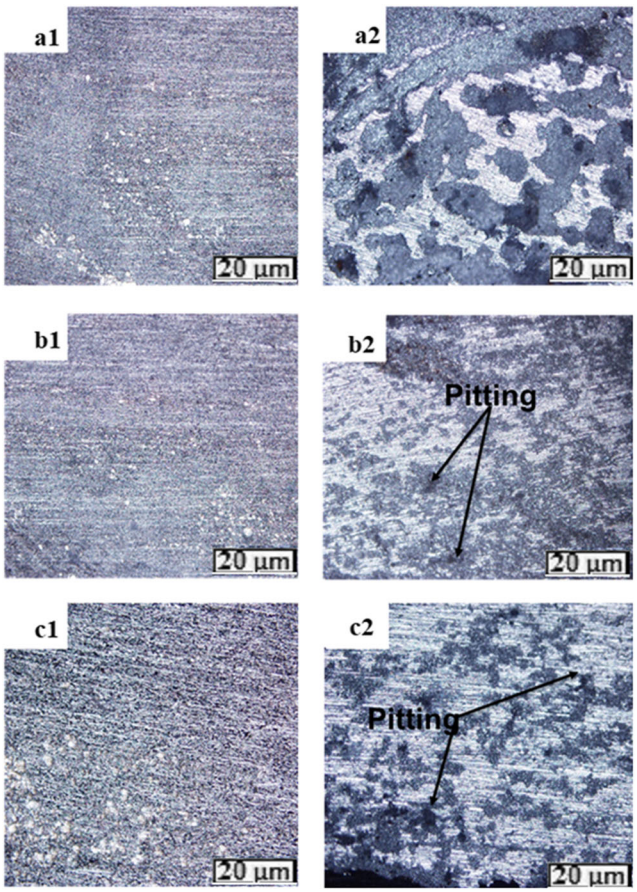

Fig. 5 Optical micrograph of FSPed samples(1-before corrosion) and corroded FSPed samples (2-after corrosion) produced at rotational and transverse speeds of (**a**) 600 rpm-70 mm/min, (**b**) 600 rpm-140 mm/min and (**c**) 600 rpm-210 mm/min

High active to passive transition region was displayed by the FSPed sample produced at a rotational speed of 600 rpm and a transverse speed of 70 mm/min as shown in Fig. 2. Less active to passive transition behaviour was displayed by the FSPed samples produced at transverse speeds of 140 mm/min and 210 mm/min when compared with the FSPed sample produced at the transverse speed of 70 mm/min. It can be seen in Fig. 2 that all the samples passivate spontaneously and go into a pseudo passive state. The corrosion potential of FSPed samples that were processed at rotational and transvers speeds of 600 rpm-140 mm/min and 600 rpm-210 mm/min are very close, and they also have lower corrosion current density making them more resistant to corrosion when compared with the base metal. The similar corrosion potential observed in FSPed samples processed at transverse speeds of 140 and 210 mm/min indicates that the uniform passive layer formed in the surface of these samples was similar. Also at the activation point, the samples have the same break point, and they show better corrosion resistance similar to the commercial pure aluminium (see Fig. 2).

The potentiodynamic polarization curves of the pure commercial aluminium and those of the FSPed Al/Ni-40Fe-10Ti composite produced at rotational speed of 800 rpm and at different transverse speeds are shown in Fig. 3. All the FSPed samples produced at rotational speed of 800 rpm also show clear active to passive transition behaviour in the 3.5% NaCl solution. The FSped samples produced at the transverse speeds of 70 mm/min and 140 mm/min also have close corrosion potential. The corrosion current density was observed at the rotational speed of 800 rpm and at transverse speeds at 70 and 140 mm/min lower when compared with the FSPed samples produced at rotational speed of 600 rpm and transverse speeds of 140 and 210 mm/min. Lower current density shows that there is less dissolution of electrons at the anode which means the corrosion resistance is improved at higher rotational speed.

The potentiodynamic polarization curves of the pure commercial aluminium and the FSPed Al/Ni-40Fe-10Ti composite produced at rotational speed of 1000 rpm and at different transverse speeds are shown in Fig. 4. The corrosion resistance of the FSPed composite was found to reduce with further increase in rotational speed. Grain refinement plays an important role in improving the passivation ability FSPed samples that helps in the formation of stable and strong passive film on metal surface [15, 16]. The improved corrosion

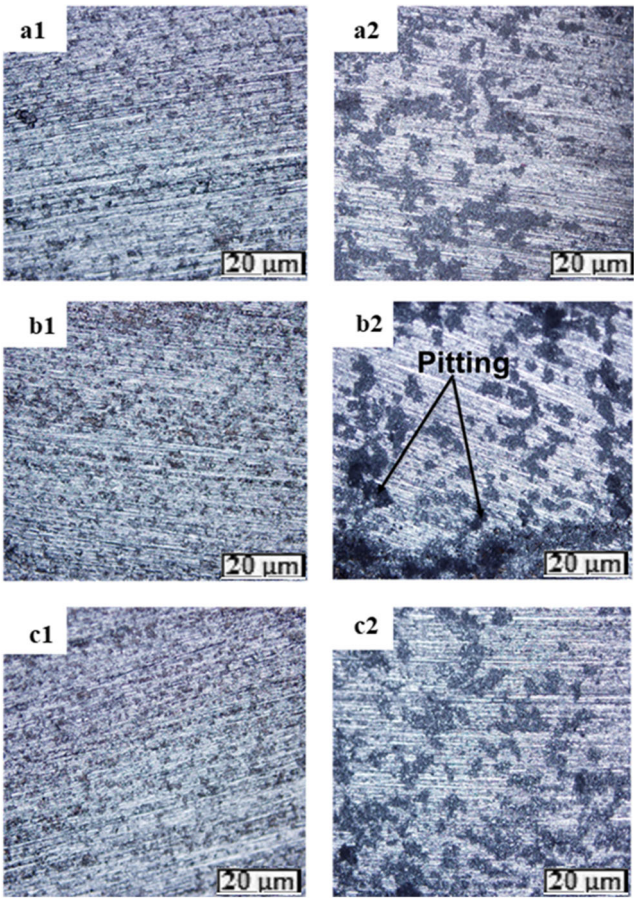

Fig. 6 Optical micrographs of FSPed samples (1-before corrosion) and corroded FSPed samples (2-after corrosion) processed at (**a**) 800 rpm-70 mm/min, (**b**) 800 rpm-140 mm/min and (**c**) 800 rpm-210 mm/min

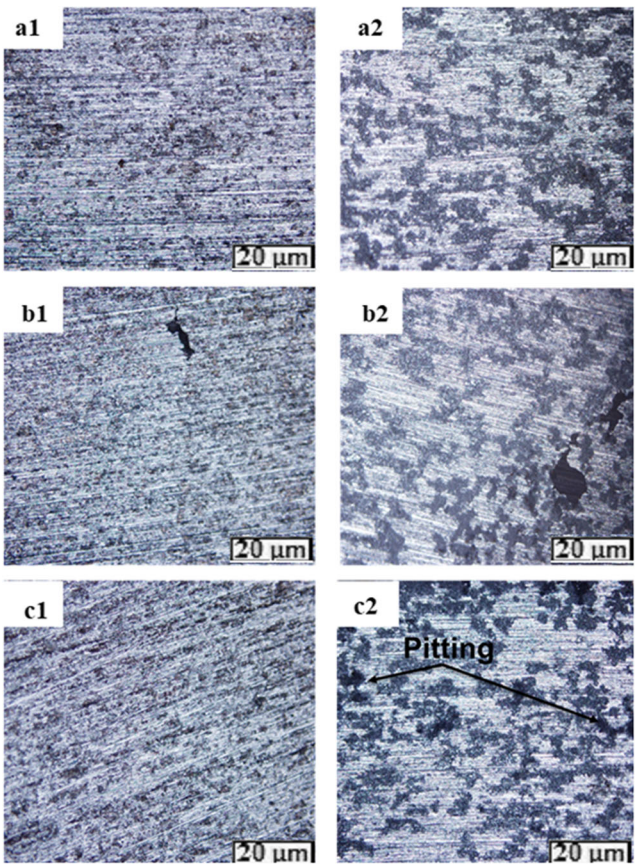

Fig. 7 Optical micrographs of FSPed samples (1-before corrosion) and corroded FSPed samples (2-after corrosion) processed at (**a**) 1000 rpm-70 mm/min, (**b**) 1000 rpm-140 mm/min and (**c**) 1000 rpm-210 mm/min

resistance observed at lower rotational speed could be attributed to the achieved grain refinement attained during FSP. The higher heat input at higher rotational speed causes grain growth which does not favour corrosion resistance. Also, the addition of the reinforcement elements Ni, Fe and Ti caused a reduction in the anodic and cathodic current densities that has resulted in improved corrosion resistance of the FSPed composite in the 3.5% NaCl solution. The FSPed sample produced at rotational speed of 600 rpm and transverse speed of 70 mm/min showed the lowest corrosion rate.

Figure 5 shows the micrograph of the FSPed samples produced at rotational speed of 600 rpm. FSPed samples before corrosion are designated as a1, b1 and c1, while FSPed samples after corrosion are designated as a2, b2 and c2, The FSPed sample processed at rotational speed of 600 rpm and at transverse speed of 70 mm/min shows less pitting corrosion (Fig. 5a2) when compared with FSPed samples produced at transverse speeds of 140 and 210 mm/min as shown in Fig. 5b2 and c2, respectively.

In Figs. 6 and 7, it is apparent that the grain boundaries were attacked in the stirred zone, and this can be attributed to the higher heat input of the FSPed samples during the friction stir processing. The generation of high heat input sensitizes the grain boundaries in the stirred zone as the FSP progresses. Pitting corrosion mainly occurs in the vicinity of the iron (Fe)-rich intermetallic particles as also discovered by Gharavia et al. in their study [17]. The X-ray diffraction (XRD) pattern of the reinforcement powder and that of the FSPed samples is shown in Fig. 8. During the initiation of the corrosion process, the Al matrix which forms the anode around the precipitate, that is, the cathode, gets preferentially dissolved. This is similar to what was observed by Sinhmar and Dwivedi in their study, and it was described as trenching [18]. As the corrosion process progresses, the precipitates began to dissolve and resulted in the pit formation due to the void that their dissolution created. Very close to the base metal, the chain of precipitates around this area causes more pit corrosion as seen in Figs. 5, 6, and 7. Trenching and pits can be observed on the corroded surfaces of friction stirred processed samples.

It can be seen in the X-ray diffraction pattern of mixed Ni-40Fe-10Ti powders (Fig. 8a) that nickel and iron have the highest percentages as represented by the highest peaks, while titanium shows the lowest peaks as a result of the mixing ratio of the three powders. The formation of an intermetallic compound Ni_4Ti_3 can also be seen during mixing. The XRD pattern of FSPed samples processed at 600 rpm with varied transverse speeds of 70, 140 and 210 mm/min as shown in Fig. 8b shows a huge difference when compared with Fig. 8a. Lesser peaks are observed in FSPed samples where the peaks show the presence of aluminium which shows that the substrate

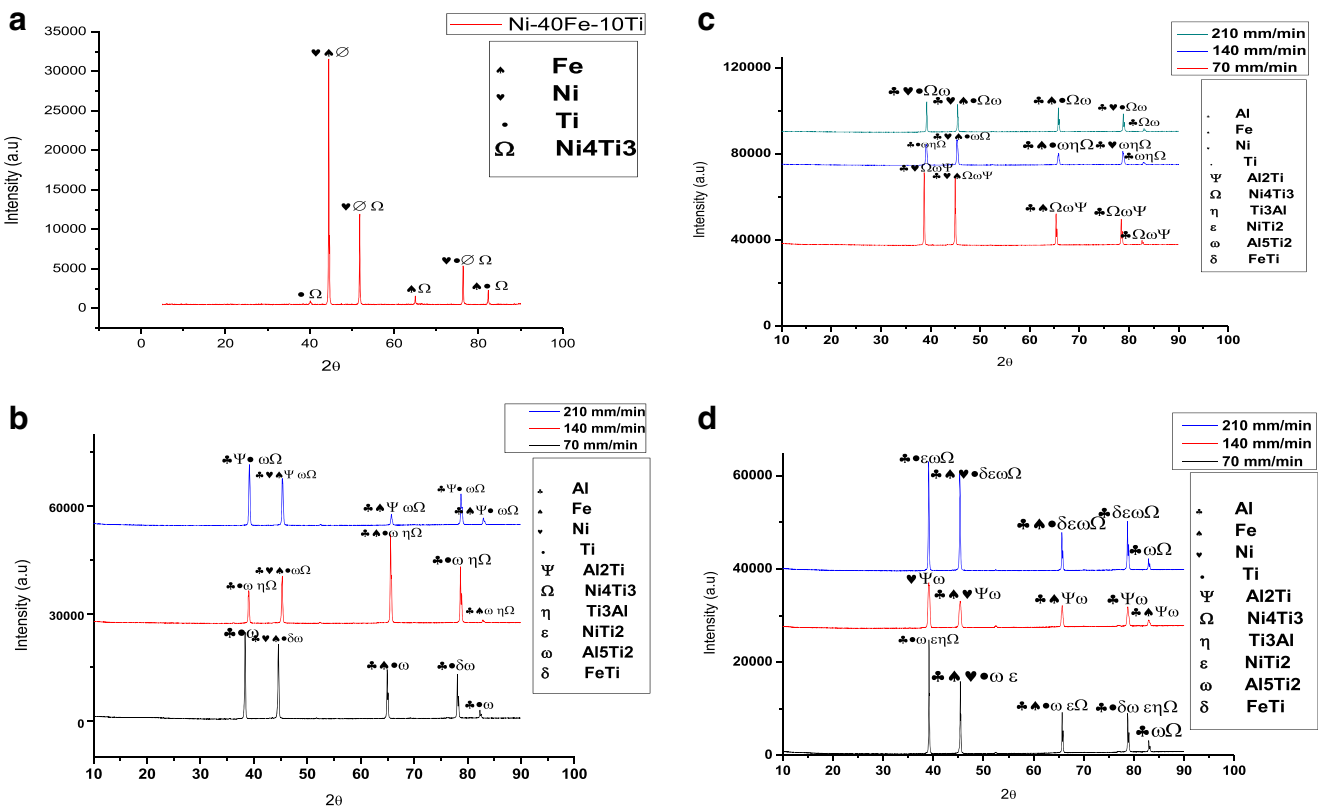

Fig. 8 X-ray diffraction pattern of (**a**) mixed powder (reinforcement powder) Ni-40Fe-10Ti, (**b**) FSPed samples processed at 600 rpm, (**c**) FSPed samples processed at 800 rpm and (**d**) FSPed samples processed at 1000 rpm

material (Al) has been mixed with the reinforcement powders during the FSP. The rotational speed and transverse speeds are seen to have activated some appreciable phase transformations. At transverse speed of 70 mm/min, it is observed from the XRD that other intermetallic compounds, FeTi and Al_5Ti_2, were also formed. With increase in transverse speed from 140 to 210 mm/min, new phases of $NiTi_2$, Ti_3Al and Al_2Ti at different peaks were also observed. At 800 rpm rotational speed and at different transverse speeds, the XRD pattern is shown in Fig. 8c. It is observed in Fig. 8c that by increasing in the rotational speed, the intermetallic compounds/phases formed at a transverse speed of 70 mm/min when compared with the sample FS processed at 600 rpm (Fig. 8b), some intermetallic compounds such as $NiTi_2$ and Al_2Ti are now present. Figure 8d further confirms that when the tool rotational speed was increased, it influences the intermetallic compounds and phases formed. It is also observed that as the transverse speed was increased from 70 to 140 mm/min, there was an increase in the concentration of Ni, Al_2Ti and Al_5Ti_2 in the first peak when compared with XRD patterns at 600 rpm (Fig. 8b) and 800 rpm (Fig. 8c). The combination of a high rotational speed with a high transverse speed has showed to improve the concentration of the reinforcement material (Ni-40Fe-10Ti) distributed along the aluminium substrate. The increase in temperature distribution or an increase in the heat generation during the FSP resulted in the formation of all these new phases.

A further look at the microstructure of the FSPed samples showed the influence of the tool rotational speed and transverse speed as it affects the heat input and the distribution of reinforcement particles due to the shattering effect of the tool rotation. The heat input caused by friction between the FSP tool and the material being processed causes plastic flow of the material during FSP. The contact between the tool shoulder and the workpiece during the FSP causes shear force to occur, which in turn resulted in the plastic flow of material in the stir zone. Figure 9 shows that as the rotational speed increases, the heat generated was increased and reinforcement powder distributions were enhanced (see Fig. 9a–i). The reinforcement particle was more evenly distributed in the nugget zone as shown in Fig. 9f–i when compared with Figs. 9a–e where the reinforcement material is seen densely populated at the top of the stirred zone (also see Figs. 10a–i). The Ni-Fe-Ti particles size decreased under the shattering effect of the high tool rotation. As reported

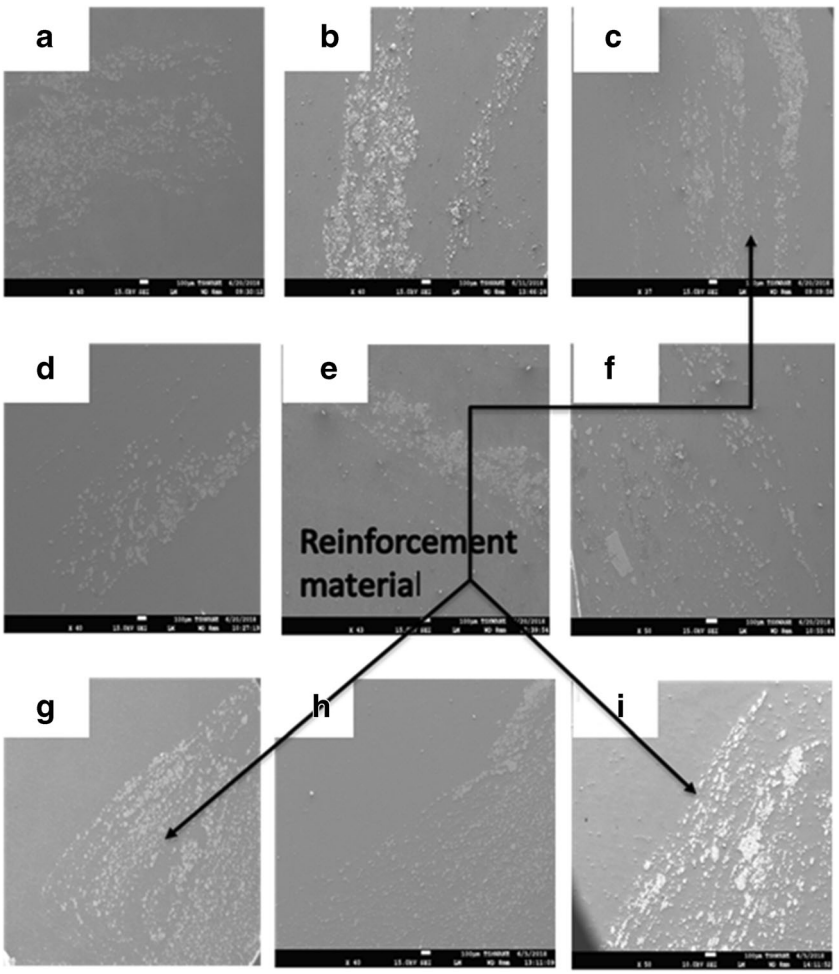

Fig. 9 SEM images of etched FSPed samples produced respectively at rotational speed and transverse speed of (**a**) 600 rpm & 70 mm/min, (**b**) 600 rpm & 140 mm/min, (**c**) 600 rpm & 210 mm/min, (**d**) 800 rpm & 70 mm/min, (**e**) 800 rpm & 140 mm/min, (**f**) 800 rpm & 210 mm/min, (**g**) 1000 rpm & 70 mm/min, (**h**) 1000 rpm & 140 mm/min and (**i**) 1000 rpm & 210 mm/min

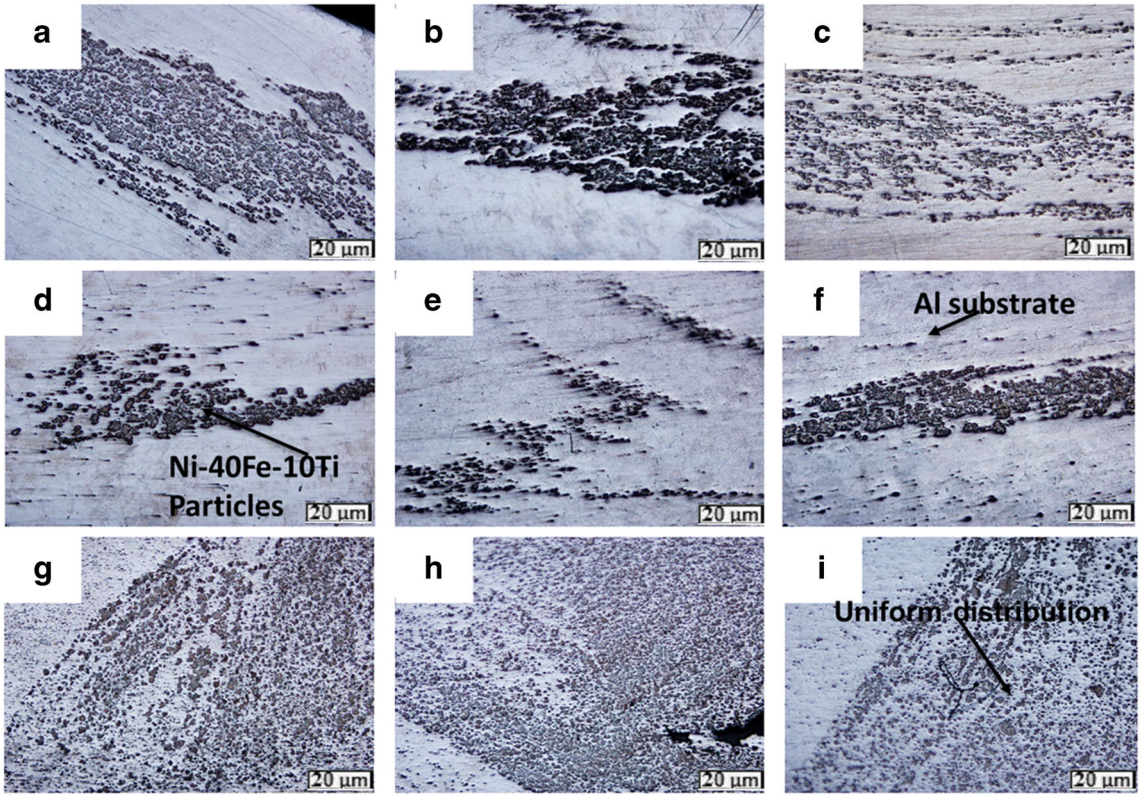

Fig. 10 Optical micrographs of FSPed samples produced respectively at rotational speed and transverse speed of (**a**) 600 rpm and 70 mm/min, (**b**) 600 rpm and 140 mm/min, (**c**) 600 rpm and 210 mm/min, (**d**) 800 rpm and 70 mm/min, (**e**) 800 rpm and 140 mm/min, (**f**) 800 rpm and 210 mm/min, (**g**) 1000 rpm and 70 mm/min, (**h**) 1000 rpm and 140 mm/min and (**i**) 1000 rpm and 210 mm/min

in the literature, the reinforcement particles increase the nucleation sites that help to break up the prior grains which restrict expansion of grain boundaries because of the pinning effect of reinforcement particles [19, 20]. Also, severe plastic deformation and dynamic recrystallization caused by FSP help to promote grain refinement of the FSPed samples. As the tool rotational speed was increased, the shearing effect of the tool caused the reinforcement particles to disperse in the matrix causing the grains to reduce and also to reduce the clustering of the reinforcement particles as seen in Fig. 9g, h, and i.

4 Conclusions

From the investigation of this study, the following conclusions can be drawn:

- Increase in the rotational speed was found to reduce corrosion resistance of FSPed Al/Ni-40Fe-10Ti composite.
- The additions of reinforcement powders of Ni, Fe and Ti to the aluminium substrate was found to contribute to improve in corrosion resistance of the FSPed Al/Ni-40Fe-10Ti composite in 3.5% NaCl.
- The sample processed at a rotational speed of 600 rpm and transverse speed of 70 mm/min had the lowest corrosion rate and, hence, the optimum processing parameter for better corrosion resistance.

Acknowledgements The authors acknowledge the provision of research facilities used in this work by the Department of Chemical, Metallurgy and Materials Science Engineering of Tshwane University of Technology. This research study is part of the joint research undertaken by a consortium of researchers from Tshwane University Technology, University of Johannesburg, Walter Sisulu University and the University of Leicester, United Kingdom, under the Industry Academic Partnership Programme (IAPP) sponsored by the Royal Academy of Engineering, United Kingdom. The content of this paper are that of the author and co-authors and not that of the sponsors of the research project.

Funding This research was supported by the National Research Foundation (NRF) of South Africa.

Data availability N/A

Compliance with ethical standards This article is in compliance with ethical standard.

Conflict of interest The authors declare that they have no conflicts of interest.

Consent for publication I hereby declare that this manuscript has not been published, and it is not under consideration in any journal.

Code availability N/A

References

1. Fuller CB, Mahoney MW, Calabrese M, Micona L (2010) Evolution of microstructure and mechanical properties in naturally aged 7050 and 7075 Al friction stir welds. Mater Sci Eng A 527: 2233–2240
2. Harrison TJ, Crawford BR, Brandt M, Clark G (2014) Modelling the effects of intergranular corrosion around a fastener hole in 7075-T651 aluminium alloy. Comput Mater Sci 84:74–82
3. Jones K, Hoeppner DW (2009) The interaction between pitting corrosion, grain boundaries, and constituent particles during corrosion fatigue of 7075-T6 aluminium alloy. Int J Fatigue 31(2009): 686–692
4. Fraker AC, Ruff AW Jr (1970) Microstructural studies of 7075 Al relation to the directional sensitivity for stress corrosion cracking. Corros Sci 10:191–195
5. Xu J, Zou B, Tao S, Zhang M, Cao X (2016) Fabrication and properties of Al2O3eTiB2eTiC/Al metal matrix composite coatings by atmospheric plasma spraying of SHS powders. J Alloys Compd 672:251–259
6. Akinlabi ET, Mahamood RM Akinlabi SA, Ogunmuyiwa E (2014) Processing parameters influence on wear resistance behaviour of friction stir processed Al-TiC composites advances in materials science and engineering. Available online at: https://doi.org/10.1155/2014/724590
7. Akinlabi ET, Mahamood RM, Akinlabi SA (2016) Advanced manufacturing techniques using laser material processing. IGI Global, Hershey
8. Akinlabi ET, Mahamood RM (2020) Solid-state welding: friction and friction stir welding processes. Springer, Cham
9. Mishra RS, Mahoney MW, McFadden SX, Mara NA, Mukherjee AK (2000) Scripta Mater 42:163–168
10. Thomas WM, Nicholas D, Needham JC, Murch MG, Smith PT, Dawes CJ (1991) Friction stir welding, International Patent Appl. No. PCT/GB92/02203 and GB Patent Application No. 9125978.8 and US Patent Application No. 5,460,317.
11. Mahmoud TS (2013) Surface modification of A390 hypereutectic Al–Si cast alloys using friction stir processing. Surf Coat Technol 228:209–220
12. Li B, Shen Y, Hu W, Luo L (2014) Surface modification of Ti–6Al–4V alloy via friction-stir processing: microstructure and dry sliding wear performance. Surf Coat Technol 239:160–170
13. Ma ZY (2008) Friction stir processing technology: a review. Metall Mater Trans A 39A:642–658
14. Chiumenti M, Cervera M, Agelet de Saracibar C, Dialami N (2013) Numerical modeling of frictional stir welding processes. Comput Methods Appl Mech Eng 254:353–369
15. Balyanov A, Kutnyakova J, Amirkhanova N, Stolyarov V, Valiev R, Liao X, Zhao Y, Jiang Y, Xu H, Lowe T (2004) Corrosion resistance of ultra fine-grained Ti. Scr Mater 51:225–229
16. Argade G, Panigrahi S, Mishra R (2012) Effects of grain size on the corrosion resistance of wrought magnesium alloys containing neodymium. Corros Sci 58:145–151
17. Gharavia F, Matoria KA, Yunusa R, Othman NK (2014) Investigation of the nugget zone corrosion behavior in friction stir welded lap joints of 6061-T6. Aluminum Alloy 17(6):1563–1574
18. Sinhmar S, Dwivedi DK (2017) Enhancement of mechanical properties and corrosion resistance of friction stir welded joint of AA2014 using water cooling. Mater Sci Eng A 684(2017):413–422
19. Zahmatkesh B, Enayati MH (2010) A novel approach for development of surface nanocomposite by friction stir processing. Mater Sci Eng A 527:6734–6740
20. Shamsipur A, Kashani-Bozorg SF, Zarei-Hanzaki A (2011) The effects of friction-stir process parameters on the fabrication of Ti/SiC nano-composite surface layer. Surf Coat Tech 206:1372–1381